Analytical prediction of the number of Bénard cells manifesting in cylindrical(axi-symmetric) and two-dimensional rectangular enclosures for a given aspect ratio

P. G. Siddheshwar *, K. M. Lakshmi, David Laroze, C. Kanchana

Posted Date: 26 September 2023

doi: 10.20944/preprints202309.1721.v1

Keywords: Aspect ratio; Cylinder; Cell width; Enclosure; Rayleigh-Bénard convection; Rectangular

Article

Analytical Prediction of the Number of Bénard Cells Manifesting in Cylindrical(Axi-Symmetric) and Two-Dimensional Rectangular Enclosures for a Given Aspect Ratio

P. G. Siddheshwar [1,*,†], K. M. Lakshmi [2,*,†], D. Laroze [3,†] and C. Kanchana [3,†]

[1] Centre for Mathematical Needs, Department of Mathematics, CHRIST (Deemed to be University), Hosur Road, Bengaluru 560029, India
[2] Department of Mathematics, School of Physical sciences, Central University of Karnataka, Kalaburagi-585367, Karnataka, India
[3] Instituto de Alta Investigación, Universidad de Tarapacá, Casilla 7D, Arica 1000000, Chile
* Correspondence: drlakshmidurgesh@gmail.com
† These authors contributed equally to this work.

Abstract: The paper reports an analytical study of two problems of Rayleigh-Bénard convection(RBC): one in a Newtonian liquid occupying an axi-symmetric cylindrical enclosure(CE) and second in a two-dimensional rectangular enclosure(RE). Linear stability analysis is employed to obtain information on the onset of convection in terms of a critical Rayleigh number, Ra, as a function of the aspect ratio, R_o. The nature and the flow structures of the convective cells, at the onset of convection, are predicted theoretically by plotting the streamlines for different values of R_o. Not so shallow$(R_o < 1$ or $R_o \ll 1)$, and very shallow enclosures$(R_o \gg 1)$ are considered. Concepts of cell-width and the wave number are respectively used in these two types of enclosures. An explicit analytical expression for the number of cells as a function of R_o is obtained theoretically. Exact prediction of the critical value of Ra, viz., Ra_c, as a function of R_o is also made. These are new findings in the case of both CE and RE. The fundamental differences between the problems of CE and RE are also highlighted.

Keywords: aspect ratio; cylinder; cell width; enclosure; Rayleigh-Bénard convection; rectangular

1. Introduction

Rayleigh-Bénard convection(RBC) is induced by the density variation in a layer of a Newtonian fluid heated from below. The fluid in the system convects when the temperature difference between the horizontal boundaries crosses a threshold value. One then says that the onset of convection has occurred. The study of onset is very important in understanding and describing the stability of the system. The RBC problem is generally studied in the following two geometries:

1. Rectangular geometry and
2. Cylindrical geometry.

Of the various regimes that one can study concerning this problem, it is the two-dimensional problem in both the geometries that can be analysed well analytically and compared. In the case of the cylindrical geometry we would require the imposition of axisymmetry for the sake of comparison with the rectangular RBC problem. In what follows we present a literature survey of such comparable problems. The main focus of this paper is on the cylindrical RBC problem with axisymmetry with the well explored two-dimensional rectangular RBC problem being used mostly for comparison and completeness. We first survey articles on RBC in a rectangular geometry[1–5]. The two-dimensional analysis of RBC in a Boussinesq fluid bounded between two horizontal free surfaces is investigated by Moore and Weiss[1]. In their linear and nonlinear studies of the problem, different values of the

 doi:10.20944/preprints202309.1721.v1

Prandtl number, Pr, and the Rayleigh number(upto 1000 times of its critical value) are considered. They found from the study that for $Pr > 1$ the heat flux is found to be maximum for cells whose width is between 1.2 to 1.4 times of its layer depth and for $Pr = 6.8$ the heat flux is maximum for square cells. Bergé and Dubois[2] presented physical reasons for the instability mechanisms in RBC. Two phenomena near and close to the critical point are presented in the framework of a mean field approach. The dynamics of the convective pattern and the selection of the wave number is considered in the case of large aspect ratio cells. Roche et al.[3] proposed a model to find side wall effects on RBC. They found that when the conductivity of the wall material is greater than the conductivity of the fluid then the wall effect is regulated by the wall number where the wall number is defined as the ratio of the empty cell conductivity to that of the conductivity of the stagnant fluid. Stevens et al.[4] investigated the influence of lateral thermal boundary conditions on heat transport in RBC using the DNS(direct numerical simulation) method. They found from the study that the heat transport is maximum for an isothermal side wall boundary condition compared to the adiabatic one. Wen et al.[5] constructed the conditional upper and lower bounds for the heat transport in RBC. The upper bound estimation is found for stress-free boundary condition and the lower bound estimate is determined for both stress-free and no-slip boundary conditions. The results show that the lower bound captures the classical result of $1/3^{rd}$ scaling of the Rayleigh number.

We now present a detailed literature survey of the cylindrical RBC problem. Liang et al.[6] numerically investigated the buoyancy driven convection in an axi-symmetric cylindrical geometry by considering temperature-dependent viscosity. They found that the temperature-dependent viscosity has no effect on the stability or the rate of convergence of the numerical methods. Stork and Müller[7] experimentally investigated axi-symmetric thermoconvective flows in circular vessels(cylinder and annulus). The critical Rayleigh number was obtained as a function of the aspect ratio(diameter to height ratio) and the annular width of the enclosure. The influence of lateral walls with various thermal conductivities and boundary wall thicknesses were examined. Charlson and Sani[8] investigated the onset of convection in an axi-symmetric cylindrical enclosure bounded by rigid boundaries using the Rayleigh-Ritz method. The aspect ratio(radius/height) in the range from 1 to 8 is considered in the study. The obtained results are validated with the experimental works of Koschmieder[9–11]. Later, Charlson and Sani[12] extended their work on axi-symmetric flow to non-axi-symmetric flows. Hébert et al.[13] simulated and experimentally studied the onset of convection and the convection pattern in a cylindrical enclosure(with no axisymmetry assumption) with aspect ratio(diameter/height) in the range:[1, 9]. They observed one and two convection rolls in the aspect ratio ranges $[1, 1.58 \pm 0.1]$ and $[1.58, 3.26 \pm 0.02]$ respectively. Wang et al.[14] numerically investigated thermal convection in a cylinder of unit aspect ratio(radius/height). Various ranges of Prandtl and Rayleigh numbers were considered in the study. The transition from a steady flow to an oscillatory flow is found to occur at small Rayleigh number and small Prandtl number. Yu et al.[15] numerically simulated the onset of convection and studied the convective pattern in a circular cylinder for intermediate values of the aspect ratio(diameter/height) in the range of [6, 20]. They found from the study that the critical Rayleigh number decreases asymptotically for an increase in the value of the aspect ratio. They also found that the mode of onset switches between two values, 1 and 0, that correspond to even and odd values respectively of the aspect ratio. Li et al.[16] numerically studied the onset of convection and the heat transport for two different values of aspect ratios(radius/height), 1 and 2, with the Prandtl number taken as 1. They found from the study that the flow patterns are symmetric for the considered two values of the aspect ratio. They also showed that the heat transport varies directly on the aspect ratio.

Analogous cylindrical RBC problems in a porous medium are also investigated by many[17–22]. Though our study does not concern a porous medium, these articles are useful in obtaining an analytical solution in the present study. Zebib[17] studied the linear stability analysis of natural convection in a porous cylinder. He showed that the asymmetric modes are the preferred modes of convection except in the range of aspect ratios(radius/height):[1.09, 1.28], where the axi-symmetric mode of

 doi:10.20944/preprints202309.1721.v1

convection is preferred. Bau and Torrance[18] investigated the onset of *RBC* in a cylindrical annuli filled with a porous medium. They considered two types of top-wall boundary conditions(permeable and impermeable) and they found that the system is more unstable in the case of the permeable boundary condition compared to the case of the impermeable one. Haugen and Tyvand[19] studied the onset of convection in a densely packed porous cylinder whose boundaries are impermeable and perfectly heat conducting. They found that the axi-symmetric mode of convection is always the preferred one. They also found that the Rayleigh number is a smooth function of the radius to height ratio in the case of the conducting boundary condition which is opposite to what is seen in the case of an insulating boundary. Bringedal et al. [20] investigated the onset of *RBC* in a cylindrical annuli with either insulating or heat conducting boundary condition. They found from the study that the effect of inner radius on onset is more significant in the case of heat conducting boundaries compared to the insulating boundary condition. The *RBC* induced in a vertical porous cylinder by subjecting its lower horizontal wall to uniform heat flux and by maintaining the upper horizontal wall with an uniform temperature is investigated analytically by Barletta and Storesletten[21]. They carried out a linear stability analysis and an analytical solution is obtained by using the Mathieu function instead of the Bessel function. Siddheshwar and Lakshmi[22] analytically studied the onset of convection and heat transport in cylindrical porous enclosures/annuli saturated by a Newtonian liquid or nanoliquids. Four different types of enclosures, viz., tall, square, shallow and very shallow, are considered in the study. They found from their study that the critical Darcy-Rayleigh number decreases with increase in the value of the aspect ratio(height/radius). Also, for the four different types of enclosures, they did a nonlinear study and showed that the tall enclosure transports maximum heat and very shallow enclosure transports the least. Recent developments in *RBC* is covered in many recent articles [23–26].

From the literature survey of the *RBC* problems in a cylindrical geometry, it is apparent that the following aspects have not been studied:

- The analytical study concerning onset of convection in cylindrical enclosures.
- Clear information about the cell aspect ratio.
- An explicit analytical expression connecting the number of cells and the aspect ratio.
- Similarities and fundamental differences between the results of cylindrical and rectangular geometries.

These aforementioned unconsidered aspects are chosen for investigation in this paper.

The present paper is organised as follows: Section 2 includes the schematic representation of an experimental set up and the complete details of the physical model considered. In section 3 we present the governing equations, boundary condition and a standard procedure of non-dimensionalisation. The quiescent basic state and perturbation solutions will also be presented. In section 4, we transform the governing equations into a product of three Helmholtz equations and then find an expression for the critical Rayleigh number using a linear stability analysis of cylindrical and rectangular *RBC* problems. In the next section on results and discussion, the information on the formation and the nature of the cells, the cell width and the wave number is presented and discussed in great detail. Explicit expressions for the number of cells and the critical Rayleigh number as a function of aspect ratio are obtained. We also list out all possible similarities and differences between the results of cylindrical and rectangular enclosures. Finally, in section 6 we report the major conclusions of the study.

2. The Physical Model

The experimental set up of Stork and Müller[7] for the thermal convection problem in a cylindrical geometry involves a copper plate of $10mm$ thickness as the lower horizontal boundary. Due to its high thermal conductivity it supports the perfect isothermal condition. A glass plate of thickness $4mm$ was considered as the upper horizontal plate which helps in making experimental observations. The thermal insulation condition of the lateral wall was achieved by considering a PVC material of

Preprints (www.preprints.org) | NOT PEER-REVIEWED | Posted: 26 September 2023 doi:10.20944/preprints202309.1721.v1

thickness $10mm$. The schematic of the same is given in Figure 1. One may similarly write down the schematic representation of the experimental set up for a rectangular enclosure.

The present analysis simulates this kind of experimental set up but with the following assumptions:

- The horizontal and lateral wall thicknesses are neglected thereby meaning that the walls are thin. Free and impermeable boundary condition is adopted in the analysis.
- Axi-symmetric convective motion is assumed in the case of cylindrical enclosure.
- The horizontal and the lateral boundaries are assumed to be perfectly isothermal and adiabatic boundaries respectively.
- The roll pattern is circular in the case of CE and straight in the case of RE.

  Liang et al.[6] in their experiment observed purely a circular roll pattern in a cylindrical enclosure of depth upto 3 cm. Hence in the present analysis, we choose maximum height of CE as 3 cm.

These assumptions make our problem idealistic and help in obtaining an analytical solution.

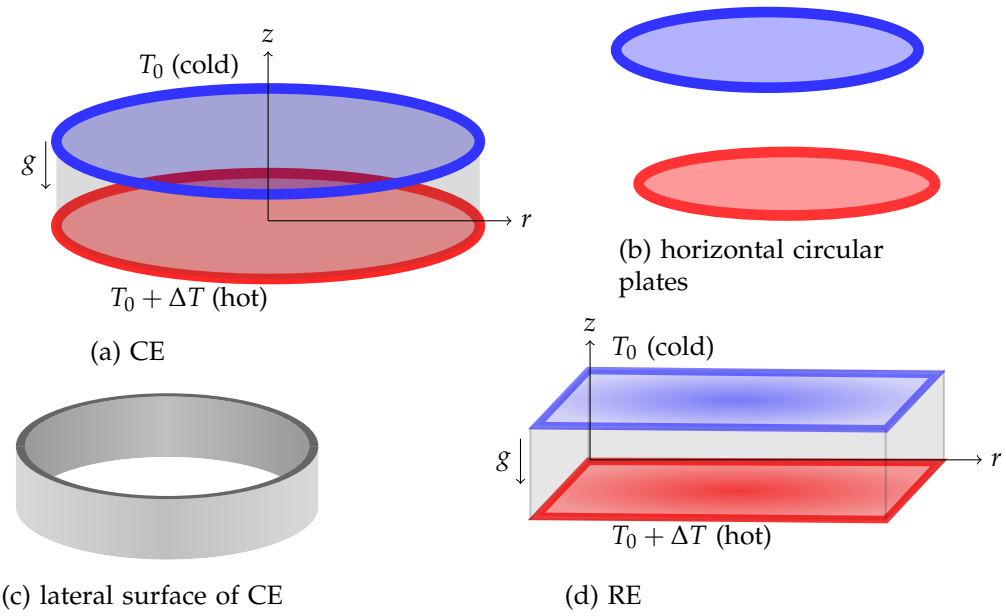

Figure 1. Schematic of the physical model for cylindrical and rectangular enclosures.

The present model considers RBC of a Newtonian liquid(water) in two different geometries(cylindrical and rectangular). We assume common notation for the cylindrical/Cartesian coordinates $(r,\ z)$. In the case of the cylinder, r is taken from the axis of the cylinder towards the lateral boundary while r is taken from the left wall towards the right wall in the case of the rectangular enclosure. In both the geometries, z is taken to be vertically upwards along the axis in the case of a cylinder and along the left wall in the case of a rectangular enclosure. The origin is taken at the bottom of the enclosure(see Figure 2). To model the problem, we have chosen CE/RE with horizontal and vertical dimensions as r_o and h, respectively. The vector $\boldsymbol{q}^* = (u,\ w)$ represents the two-dimensional velocity field. The temperature field is taken as $T = T(r,\ z,\ t)$, where t denotes the time. The boundaries of the CE/RE are assumed to be impermeable. The lower boundary, $z = 0$, is maintained at the constant higher temperature, $T = T_0 + \Delta T(\Delta T > 0)$, compared to the upper boundary temperature of $T = T_0$, where ΔT is the temperature difference. The RBC cell forms in the system due to the buoyancy effect arising due to the temperature difference between the horizontal boundaries. The lateral boundaries($r = r_0$ in CE and $r = 0,\ r_0$ in RE) are perfectly insulated.

Preprints (www.preprints.org) | NOT PEER-REVIEWED | Posted: 26 September 2023 doi:10.20944/preprints202309.1721.v1

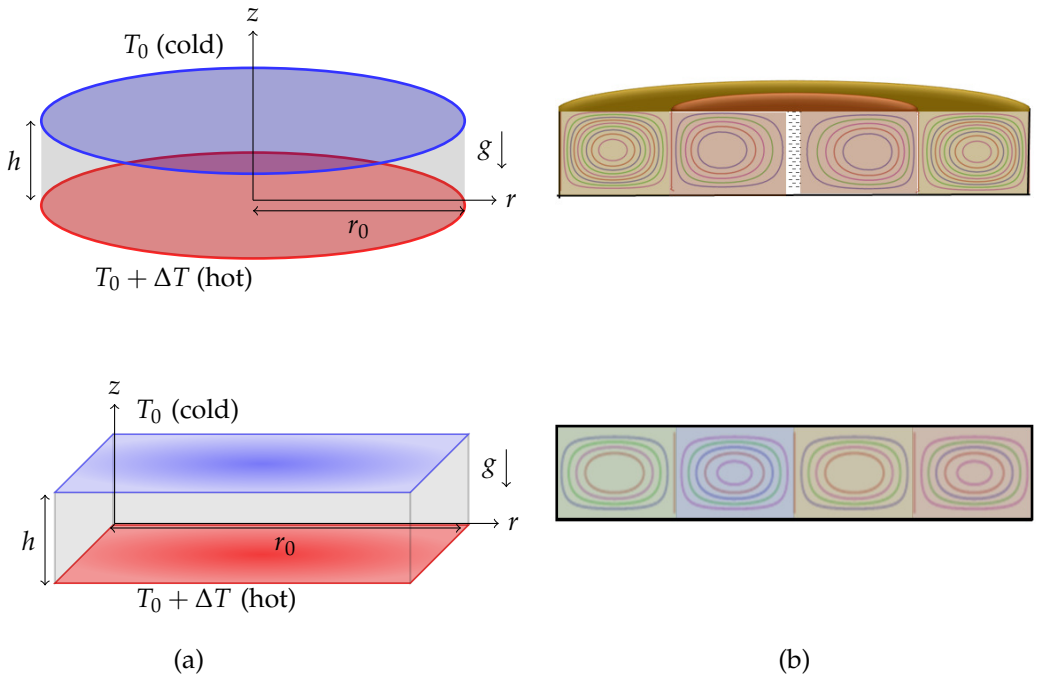

Figure 2. Schematic representation of a cylindrical and rectangular enclosures: (a) Physical representation and (b) Cross-sectional representation.

3. Mathematical Model

The conservation laws(mass, linear momentum and energy) under the Oberbeck-Boussinesq approximation are given by

$$\frac{\partial u}{\partial r} + \gamma \frac{u}{r} + \frac{\partial w}{\partial z} = 0, \tag{1}$$

$$\rho_0 \frac{\partial \boldsymbol{q}^*}{\partial t} = -\nabla P + \mu \nabla^2 \boldsymbol{q}^* + \left[\rho_0 - \rho_0 \beta \left(T - T_0\right)\right] \boldsymbol{g}, \tag{2}$$

$$\frac{\partial T}{\partial t} + \left(\boldsymbol{q}^* \cdot \nabla\right) T = \chi \nabla^2 T, \tag{3}$$

where $\nabla = \frac{\partial}{\partial r}\hat{e_r} + \frac{\partial}{\partial z}\hat{e_z}$ and $\nabla^2 = \frac{\partial^2}{\partial r^2} + \frac{\gamma}{r}\frac{\partial}{\partial r} + \frac{\partial^2}{\partial z^2}$. The parameter γ in equation (1) and in ∇^2 represents the curvature parameter. It assumes the values 1 and 0 respectively in the problems of cylindrical and rectangular enclosures. The quantities $(\rho_0,\ \mu,\ \beta,\ \chi,\ \boldsymbol{g})$ denote the density, the dynamic viscosity, the thermal expansion coefficient, the thermal diffusivity and the acceleration due to gravity, respectively. The term P in equation (2) represents the dynamic pressure which shall be eliminated by operating $\nabla \times (\nabla \times \cdots)$ on equation (2). This procedure yields the momentum equation in z-component as:

$$\rho_0 \frac{\partial}{\partial t}(\nabla^2 w) = \mu \nabla^4 w + (\rho_0 \beta) g \nabla_1^2 T. \tag{4}$$

Here $\nabla_1^2 = \frac{\partial^2}{\partial r^2} + \frac{\gamma}{r}\frac{\partial}{\partial r}$ denotes the horizontal Laplacian operator.

In what follows, we shall work with non-dimensional variables $(\Theta,\ \boldsymbol{q} = (U, W),\ (R, Z),\ \tau)$ for temperature, velocity, length and time. The scaling chosen for non-dimensionalization of $(T,\ \boldsymbol{q}^* =$

Preprints (www.preprints.org) | NOT PEER-REVIEWED | Posted: 26 September 2023 doi:10.20944/preprints202309.1721.v1

$(u, w),\ (r, z),\ t)$ is $\Delta T,\ \frac{\chi}{h},\ h$ and $\frac{h^2}{\chi}$. On scaling equations (1), (4) and (3), we get the dimensionless governing equations in the form:

$$\frac{\partial U}{\partial R} + \gamma\frac{U}{R} + \frac{\partial W}{\partial Z} = 0, \tag{5}$$

$$\frac{1}{Pr}\frac{\partial}{\partial \tau}(\nabla^2 W) = \nabla^4 W + Ra\nabla_1^2\Theta, \tag{6}$$

$$\frac{\partial \Theta}{\partial \tau} + (\boldsymbol{q}\cdot\nabla)\Theta = \nabla^2\Theta. \tag{7}$$

In equations (5)-(7), $\nabla^2 = \frac{\partial^2}{\partial R^2} + \frac{\gamma}{R}\frac{\partial}{\partial R} + \frac{\partial^2}{\partial Z^2}$ and $\nabla_1^2 = \frac{\partial^2}{\partial R^2} + \frac{\gamma}{R}\frac{\partial}{\partial R}$. The non-dimensional parameters, $Pr = \frac{\mu}{\rho_0\chi}$ and $Ra = \frac{\rho_0\beta g\Delta T h^3}{\mu\chi}$, respectively are the Prandtl and the Rayleigh numbers.

Initially, heat transport in the system is only in the form of conduction in the vertical direction. Thus, at the quiescent basic state, the temperature field takes the form $\Theta_b(Z) = \Theta_0 + 1 - Z$.

We now perturb the temperature and the velocity fields with small perturbations $(\Theta',\ \boldsymbol{q}')$ and so we take:
$\Theta = \Theta_b(Z) + \Theta'(R, Z, \tau),\ \boldsymbol{q} = \boldsymbol{q}'(R, Z, \tau)$.
The above perturbation transforms the governing equations (5)-(7) to

$$\frac{\partial U}{\partial R} + \gamma\frac{U}{R} + \frac{\partial W}{\partial Z} = 0, \tag{8}$$

$$\frac{1}{Pr}\frac{\partial}{\partial \tau}(\nabla^2 W) = \nabla^4 W + Ra\nabla_1^2\Theta, \tag{9}$$

$$\frac{\partial \Theta}{\partial \tau} + (\boldsymbol{q}\cdot\nabla)\Theta - W = \nabla^2\Theta. \tag{10}$$

In equations (8)-(10), we have omitted the primes for simplicity and the equations are solved subject to the following stress-free, isothermal horizontal and stress-free, adiabatic vertical boundary conditions as mentioned in section 2 :

$$\begin{aligned} W = \frac{\partial^2 W}{\partial Z^2} = \Theta = 0 \text{ at } Z = 0,\ 1,\ 0 \le R \le R_o, \\ U = R\frac{\partial^2 U}{\partial R^2} + \gamma\frac{\partial U}{\partial R} = \frac{\partial \Theta}{\partial R} = 0 \text{ at } R = R_o,\ 0 \le Z \le 1. \end{aligned} \tag{11}$$

Here $R_o = \frac{r_o}{h}$ represents the aspect ratio. After obtaining the dimensionless form of the governing equations and the boundary conditions, we now proceed to carry out the linear stability analysis in both CE/RE to find the threshold Rayleigh number at which the onset of convection occurs.

4. Linear Stability Analysis

The linearised form of the vorticity and the energy equations in the steady state are given by:

$$\nabla^4 W + Ra\nabla_1^2\Theta = 0, \tag{12}$$

$$\nabla^2\Theta + W = 0. \tag{13}$$

Decoupling of W and Θ from the above equations yields the following two sixth-order equations for W and Θ:

$$\nabla^6 W - Ra\nabla_1^2 W = 0, \tag{14}$$

$$\nabla^6\Theta - Ra\nabla_1^2\Theta = 0. \tag{15}$$

Preprints (www.preprints.org) | NOT PEER-REVIEWED | Posted: 26 September 2023 doi:10.20944/preprints202309.1721.v1

The $Z-$dependent part of the variable separable eigenfunctions corresponding to the roll planform(velocity) and isothermal conditions(temperature) are of the form $\sin[\pi Z]$. Thus we take

$$W(R,\ Z) = W^*(R)\sin[\pi Z],\ \Theta(R,\ Z) = \Theta^*(R)\sin[\pi Z]. \tag{16}$$

In view of this, for the purpose of calculation we require $\dfrac{\partial^2}{\partial Z^2}$ by $-\pi^2$ and ∇^2 by ∇^{*^2}, where $\nabla^{*^2} = \nabla_1^2 - \pi^2$ or $\nabla_1^2 = \nabla^{*^2} + \pi^2$. With this, the equations (14) and (15) result in:

$$\nabla^{*^6}W^* - Ra\nabla^{*^2}W^* - Ra\pi^2 W^* = 0, \tag{17}$$
$$\nabla^{*^6}\Theta^* - Ra\nabla^{*^2}\Theta^* - Ra\pi^2\Theta^* = 0. \tag{18}$$

Let us factorise equations (17) and (18) as follows:

$$(\nabla^{*^2} + \mathfrak{a}^*)(\nabla^{*^2} + \mathfrak{b}^*)(\nabla^{*^2} + \mathfrak{c}^*)W^* = 0, \tag{19}$$
$$(\nabla^{*^2} + \mathfrak{a}^*)(\nabla^{*^2} + \mathfrak{b}^*)(\nabla^{*^2} + \mathfrak{c}^*)\Theta^* = 0. \tag{20}$$

where $\mathfrak{a}^*$, $\mathfrak{b}^*$ and $\mathfrak{c}^*$ are to be determined. On multiplying together the three factors in equation (19), we get

$$\begin{aligned}\nabla^{*^6}W^* + (\mathfrak{a}^* + \mathfrak{b}^* + \mathfrak{c}^*)\nabla^{*^4}W^* + \\ (\mathfrak{a}^*\mathfrak{b}^* + \mathfrak{b}^*\mathfrak{c}^* + \mathfrak{c}^*\mathfrak{a}^*)\nabla^{*^2}W^* + \mathfrak{a}^*\mathfrak{b}^*\mathfrak{c}^*W^* = 0.\end{aligned} \tag{21}$$

Now on comparing equations (17) and (21), we get the following relations connecting $\mathfrak{a}^*$, $\mathfrak{b}^*$ and $\mathfrak{c}^*$:

$$\mathfrak{a}^* + \mathfrak{b}^* + \mathfrak{c}^* = 0, \tag{22}$$
$$\mathfrak{a}^*\mathfrak{b}^* + \mathfrak{b}^*\mathfrak{c}^* + \mathfrak{c}^*\mathfrak{a}^* = -Ra, \tag{23}$$
$$\mathfrak{a}^*\mathfrak{b}^*\mathfrak{c}^* = -Ra\pi^2. \tag{24}$$

In what follows we shall first obtain the solution for the equation (20) and then similarly solve the equation (19). The eigenfunction for the temperature field should satisfy any one of the following three Helmholtz equations:

$$(\nabla^{*^2} + \mathfrak{a}^*)\Theta^* = 0,\ (\nabla^{*^2} + \mathfrak{b}^*)\Theta^* = 0,\ (\nabla^{*^2} + \mathfrak{c}^*)\Theta^* = 0. \tag{25}$$

The solution of the Helmholtz equations in (25) is different in cylindrical and rectangular *RBC* problems. Hence it shall be discussed in two different sub-sections below.

4.1. Expression for the Rayleigh number in the cylindrical RBC problem (the case of $\gamma = 1$)

The solution of equation (25) in cylindrical coordinates is:

$$\begin{aligned}\Theta_1 &= A_0 J_0[\mathfrak{a}R]\sin[\pi Z], \\ \Theta_2 &= A_0' J_0[\mathfrak{b}R]\sin[\pi Z], \\ \Theta_3 &= A_0'' J_0[\mathfrak{c}R]\sin[\pi Z],\end{aligned} \tag{26}$$

where J_0 is the Bessel function of the first kind and of zeroth order, and $\mathfrak{a} = \sqrt{\mathfrak{a}^* - \pi^2}$, $\mathfrak{b} = \sqrt{\mathfrak{b}^* - \pi^2}$, $\mathfrak{c} = \sqrt{\mathfrak{c}^* - \pi^2}$, and A_0, A_0' and A_0'' are the infinitesimal amplitudes of convection. Among Θ_1, Θ_2 and Θ_3, we consider Θ_1 but call it as Θ in our further analysis. Similarly, we obtain W_1, W_2 and W_3 as solutions and consider only W_1 further on but with the name W and is given by:

$$W = B_0 J_0[\mathfrak{a}R]\sin[\pi Z], \tag{27}$$

Preprints (www.preprints.org) | NOT PEER-REVIEWED | Posted: 26 September 2023 doi:10.20944/preprints202309.1721.v1

where B_0 is an infinitesimal amplitude.

Next we find the critical Rayleigh number in terms of $\mathfrak{a}$, $\mathfrak{b}$ and $\mathfrak{c}$ and to that end we make use of the relations:

$$\mathfrak{a}^* = \mathfrak{a}^2 + \pi^2, \ \mathfrak{b}^* = \mathfrak{b}^2 + \pi^2, \ \mathfrak{c}^* = \mathfrak{c}^2 + \pi^2 \tag{28}$$

in equations (22) and (24). In terms of $\mathfrak{a}^2$, $\mathfrak{b}^2$ and $\mathfrak{c}^2$, the obtained relations are:

$$\mathfrak{a}^2 + \mathfrak{b}^2 + \mathfrak{c}^2 = -3\pi^2, \tag{29}$$

$$(\mathfrak{a}^2 + \pi^2)(\mathfrak{b}^2 + \pi^2)(\mathfrak{c}^2 + \pi^2) = -Ra\pi^2. \tag{30}$$

On substituting equation (28) into equation (23) and using equation (24), we obtain one more equation connecting $\mathfrak{a}$, $\mathfrak{b}$, $\mathfrak{c}$:

$$\mathfrak{a}^2\mathfrak{b}^2\mathfrak{c}^2 = -\pi^6. \tag{31}$$

Now on completing the multiplication in equation (30), we get

$$\mathfrak{a}^2\mathfrak{b}^2\mathfrak{c}^2 + \mathfrak{a}^2(\mathfrak{b}^2 + \mathfrak{c}^2)\pi^2 + \mathfrak{b}^2\mathfrak{c}^2\pi^2 + (\mathfrak{a}^2 + \mathfrak{b}^2 + \mathfrak{c}^2)\pi^4 + \pi^6 = -Ra\pi^2. \tag{32}$$

From equations (29) and (31), we may write

$$\mathfrak{b}^2 + \mathfrak{c}^2 = -3\pi^2 - \mathfrak{a}^2, \tag{33}$$

$$\mathfrak{b}^2\mathfrak{c}^2 = -\frac{\pi^6}{\mathfrak{a}^2}. \tag{34}$$

Using equations (29), (31), (33) and (34) in equation (32), and rearranging the resulting equation for Ra, we get

$$Ra = \frac{(\mathfrak{a}^2 + \pi^2)^3}{\mathfrak{a}^2}. \tag{35}$$

Clearly, Ra is dependent on $\mathfrak{a}$ and to determine $\mathfrak{a}$ we make use of the adiabatic temperature boundary condition at the radial wall, i.e., $\frac{\partial \Theta}{\partial R} = 0$ at $R = R_o$. With this condition, the Θ solution in equation (26) gives us the constraint on $\mathfrak{a}$ as follows:

$$J_1[\mathfrak{a}R_o] = 0. \tag{36}$$

For each value of R_o, there are infinitely many solutions for $\mathfrak{a}$ which satisfy the condition (36). Among these values of $\mathfrak{a}$, the particular value which minimizes the Rayleigh number is the required value of $\mathfrak{a} = \mathfrak{a}_c$. We defer the naming of $\mathfrak{a}_c$ as the critical wave number and the reason shall become apparent in the section 5.

4.2. Expression for the Rayleigh number in the rectangular RBC problem (the case of $\gamma = 0$)

The solution of the representative Helmholtz equation in (25) in Cartesian coordinates is given by

$$\Theta_1 = A_0 \cos[\mathfrak{a}R] \sin[\pi Z]. \tag{37}$$

Similar arguments to that used in section 4.1 are applied here to obtain the solution for Θ and W:

$$\Theta = A_0 \cos[\mathfrak{a}R] \sin[\pi Z], \tag{38}$$

$$W = B_0 \cos[\mathfrak{a}R] \sin[\pi Z], \tag{39}$$

where A_0 and B_0 are infinitesimal amplitudes of convection.

The expression of the Rayleigh number takes the same form as that given in equation (35) but with a different value of $\mathfrak{a}$. The adiabatic temperature boundary condition, $\frac{\partial \Theta}{\partial R} = 0$ at $R = R_o$, results in the $\mathfrak{a}$-constraint as:

$$\sin[\mathfrak{a}R_o] = 0. \tag{40}$$

Preprints (www.preprints.org) | NOT PEER-REVIEWED | Posted: 26 September 2023 doi:10.20944/preprints202309.1721.v1

On simplification, we obtain

$$\mathfrak{a} = \frac{k\pi}{R_o}, \tag{41}$$

where $k = 1, 2, 3, \cdots$. The value of k which minimizes the Rayleigh number is the required value of k in $\mathfrak{a}$. We call it as $\mathfrak{a}_c = \frac{k_c\pi}{R_o}$. With the definition of $\mathfrak{a}_c$, the critical Rayleigh number now takes the form:

$$Ra_c = \pi^4 \frac{\left[(k_c/R_o)^2 + 1\right]^3}{(k_c/R_o)^2}. \tag{42}$$

Having obtained the expressions for the Rayleigh number in cylindrical and rectangular *RBC* problems, in the section 5 we discuss the results of the investigation.

5. Results and Discussion

Analytical study of *RBC* in both cylindrical and rectangular enclosures(CE/RE) is carried out. The coupled simultaneous equations (12) and (13) governing the problem are transformed to two decoupled equations each containing the product of three Helmholtz equations(see equations (19) and (20)). The separable solution of the Helmholtz equation in cylindrical and rectangular *RBC* problems include a combination of Bessel and trigonometric functions and purely trigonometric functions respectively. Various range of values of aspect ratio, $R_o = \frac{r_o}{h}$, are considered in the study to cover the results of shallow and very shallow enclosures. We now move on to discuss the results of the paper.

The aspects of the axi-symmetric cylindrical *RBC* problem to be discussed are:

1. Understanding the nature of convecting cells, the formation of cells, and the need for considering the concept of cell width in the case of not-so-large values of R_o.
2. Providing explicit information about the connection between the aspect ratio and the number of cells.

In a few articles, the quantity $\mathfrak{a}$ in equation (35) is termed as the wave number [19,20,22] and regarding this we have the following observation to make:

For systems with not so large R_o, limited number of convection cells can be seen and hence symmetricity cannot be defined which thereby means that we cannot define a wave number. We will hence have to consider the concept of a cell-width. Hence, in what follows we prefer to use the terminology cell-width when R_o is not so large and the terminology wave number otherwise. we discuss more on this later in this section. Next, we discuss about the procedure followed to obtain the expression for the number of cells in terms of R_o.

5.1. Expression of the critical Rayleigh number

From equation (36), it is clear that $\mathfrak{a}$ is dependent on R_o. For each value of R_o, the constraint produces different values of $\mathfrak{a}_c$. To determine $\mathfrak{a}_c$ it is better to make the substitution $p = \mathfrak{a}R_o$ in equations (35) and (36). These equations then take the form:

$$Ra(R_o, p(R_o)) = \frac{\left[(p/R_o)^2 + \pi^2\right]^3}{(p/R_o)^2}, \tag{43}$$

$$J_1[p] = 0. \tag{44}$$

It is known that the constraint (44) has infinite roots. We name these roots as $p_k (k = 1,\ 2,\ 3, \cdots)$. We arrange these roots such that $p_1 < p_2 < p_3 < \cdots$. For a given value of R_o, p_1 is not necessarily the value of p(called p_c) that gives Ra_c. For different ranges of R_o, p_c can be p_1 or p_2 or p_3 or $\cdots$. This information is recorded in Table 1.

Preprints (www.preprints.org) | NOT PEER-REVIEWED | Posted: 26 September 2023 doi:10.20944/preprints202309.1721.v1

Table 1. The ranges of aspect ratio, R_o with the corresponding values of k and p.

R_o	k	$p_c = p_k$
[0.8, 2.37)	1	3.83171
[2.37, 3.82)	2	7.01559
[3.82, 5.26)	3	10.1735
[5.26, 6.68)	4	13.3237
[6.68, 8.1)	5	16.4706
[8.1, 9.52)	6	19.6159

Having obtained $p_c(R_o)$, we may now calculate Ra_c from equation (43) with p replaced by p_c. This procedure gives us

$$Ra_c(R_o, p_c(R_o)) = \frac{\left[(p_c/R_o)^2 + \pi^2\right]^3}{(p_c/R_o)^2}. \tag{45}$$

At this stage we note that we have just obtained an expression for $Ra_c(R_o)$.

5.2. Plotting of the stream function to have a good idea on the number of cells manifesting for a given R_o

From the tabulated values of Table 1, intuition tells us that k actually is the number of cells(see Table 1). In the analysis that follows, we consider this particular aspect. Having obtained p_c and Ra_c for different values of R_o, the next task in the paper is to get an expression for the number of cells, k, in terms of R_o. To arrive at this expression, we first plot the stream function for different values of R_o. We know that

$$W = \frac{1}{R}\frac{\partial \psi}{\partial R}, \tag{46}$$

where ψ denotes the stream function. Substituting equation (27) into equation (46)(with $\mathfrak{a}$ replaced by p_c/R_o), and integrating the resulting equation with respect to R, we get the following expression for ψ:

$$\psi = \mathcal{A}\frac{p_c/R_o}{\left[(p_c/R_o)^2 + \pi^2\right]^2} Ra\ R J_1\left[\frac{p_c}{R_o}R\right] \sin[\pi Z], \tag{47}$$

where $\mathcal{A}$ is an arbitrary constant and the constant of integration does not appear in equation (47) since the boundary is also a streamline.

Figure 3 essentially reiterates the results of Table 1 but with the additional information that k, in fact, represents the number of cells. For plotting Figure 3a, we consider a representative value of $R_o = 1 \in [0.8,\ 2.37)$. Clearly one cell manifests here. For other values of R_o within the above interval, it is just one cell that manifests. Regarding this solitary cell we note that it performs anticlockwise circulation. Further, the cell is not equidistant from the axis of the cylinder and its lateral surface. Between the axis of the cylinder and the outermost left boundary of the circulating solitary cell, the fluid is stagnant. This stagnant region is covered by the innermost circular roll. For plotting Figure 3b, we have considered $R_o = 2.37 \in [2.37,\ 3.82)$. As in Figure 3a, the first cell circulates anticlockwise while the new cell that forms closer to the lateral surface of the cylinder circulates clockwise. Proceeding further and considering values of R_o in the remaining four ranges mentioned in Table 1, we get a sequence of anticlockwise and clockwise circulating cells and the exact number of cells showing up depends on the choice of R_o. The particular values of R_o chosen in Figure 3 are representative values from the six ranges of R_o mentioned in Table 1.

Next, we provide some more information on the computations that have been performed. For this we single out the value $R_o = 42$. In this case too, the cells formed at a distance from the axis with the first circulating cell being anticlockwise, the second being clockwise and the other cells circulating in alternate directions as we move towards the lateral surface of the cylinder. An important observation, however, from the computation done in the paper is that the first cell stands out as being different from the other cells. Except the first cell, we observe a symmetry in the horizontal dimension of the

Preprints (www.preprints.org) | NOT PEER-REVIEWED | Posted: 26 September 2023 doi:10.20944/preprints202309.1721.v1

other cells. The vertical dimension of the other cells, however, differ from each other. It was found that as R_o increases, the height of the cells increase with the tallest found close to the lateral surface of the cylinder. Yet another observation that can be made in regard to the formation of the cells is that beyond the first cell(for $R_o > 2.36$) increase in the number of cells happens for an increase approximately by 1.42 in R_o. This estimation gets accurate for values of $R_o > 5.26$.

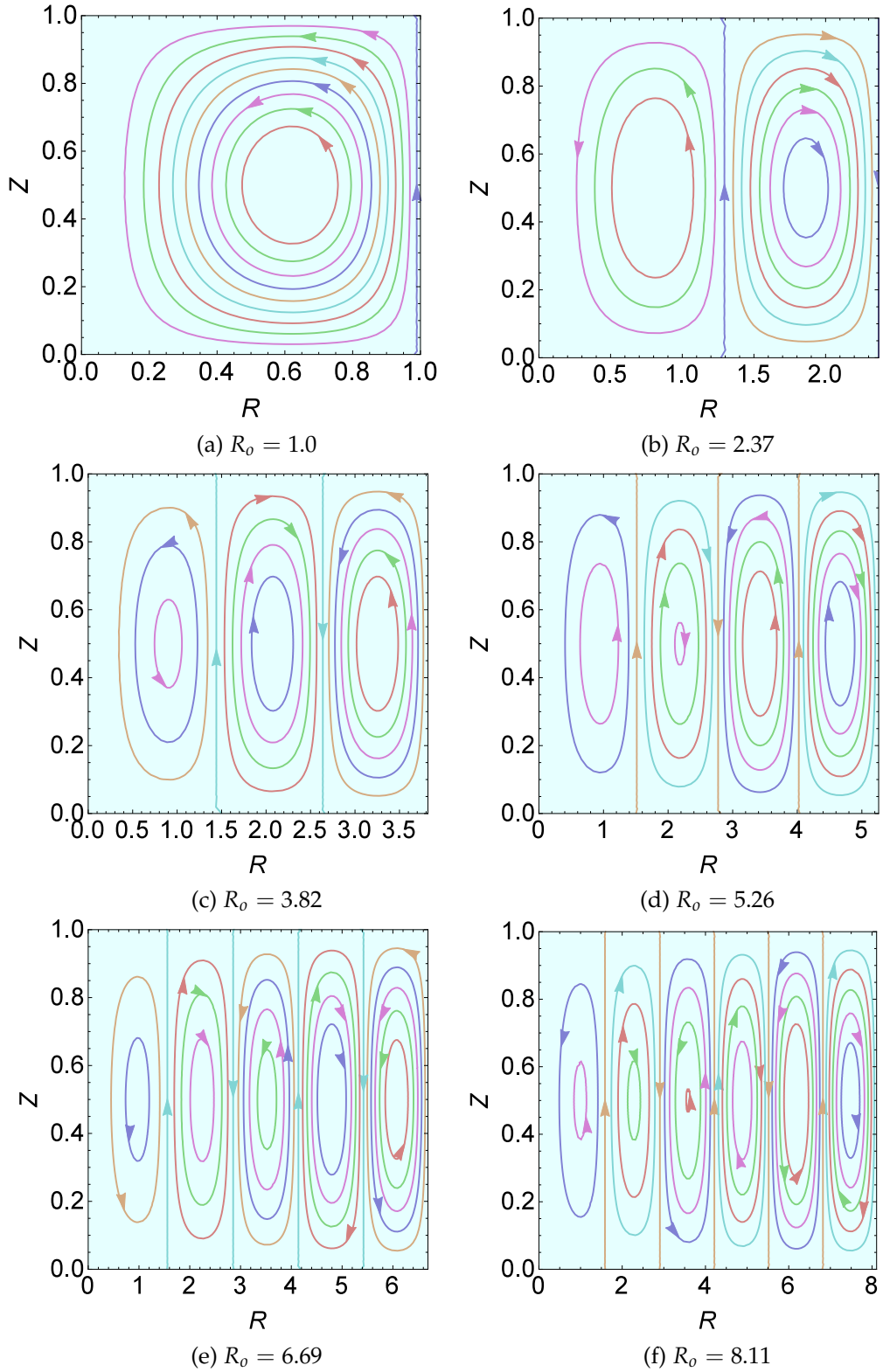

(a) $R_o = 1.0$ (b) $R_o = 2.37$

(c) $R_o = 3.82$ (d) $R_o = 5.26$

(e) $R_o = 6.69$ (f) $R_o = 8.11$

Figure 3. Plot of streamlines, Ψ, versus the radius to height ratio, R, for different values of aspect ratio, R_o.

Preprints (www.preprints.org) | NOT PEER-REVIEWED | Posted: 26 September 2023 doi:10.20944/preprints202309.1721.v1

5.3. The concepts of cell-width and the wave number

In the discussion that follows we consider two ranges of values of R_o:

1. $0.8 \leq R_o < 42$(not very shallow cylindrical enclosures):

   For these cylindrical enclosures, we find that there are finite number of cells whose structure is very much different from each other and hence symmetricity cannot be observed between the cells. Thus, the concept of wave number is inapplicable. In these situations, we will have to make use of the concept of the cell-width which is essentially the width of one cell.
2. $42 < R_o < \infty$(very shallow cylindrical enclosures):

   In these enclosures, the cells structure seems more or less symmetric to the classical rectangular RB cells except for the first cell that forms around the axis of the cylinder but at a distance from the axis. In this case, we note that there is a finite cylindrical space around the axis in which the fluid is static(stagnant zone or no-cell zone). Just next to this static zone, convective activity is seen. The width of this first convective activity is different from the structure of subsequent cells that form when we increase R_o. Even though we have noted that the cylindrical RB cells are similar to the rectangular RB cells when R_o is large, it is extremely important to note that there is one fundamental difference. We can easily observe that the height of the cylindrical RB cell is least near the axis of the cylinder and takes a maximum height in a region very close to the vertical curved surface of the cylinder. Yet another important observation we have made is that the width of the first cell is always not equal to that of the other cells. This is in contrast to what we observe in the case of rectangular RBC wherein cells that form are such that they are of the same size(see Figure 4).

From the above proceedings we next consider the following evident aspects of cylindrical RBC:

1. For not so large values of R_o we cannot use the concept of wave-length. We will have to make use of the concept of a cell-width.
2. In the case of very large R_o, however, the concept of wave number applies but only in regions beyond the first cell.

For very large R_o wherein the concept of wave number applies, when we refer to one wave-length we refer to a pair of counter rotating cells and in the case of small/moderate values of R_o, the cell-width refers to the horizontal dimension of one cell. An other important point to always remember in the case of the considered RBC cells is that the concepts of cell-width, wave-length and wave number, whichever is applicable, are concepts that have to do with the horizontal dimension of the RB cell and not on the vertical dimension of such a cell. It is well known that at large values of the aspect ratio the axi-symmetric convection breaks down. In this case, the results of CE shall be obtained from the classical RBC problem.

Preprints (www.preprints.org) | NOT PEER-REVIEWED | Posted: 26 September 2023 doi:10.20944/preprints202309.1721.v1

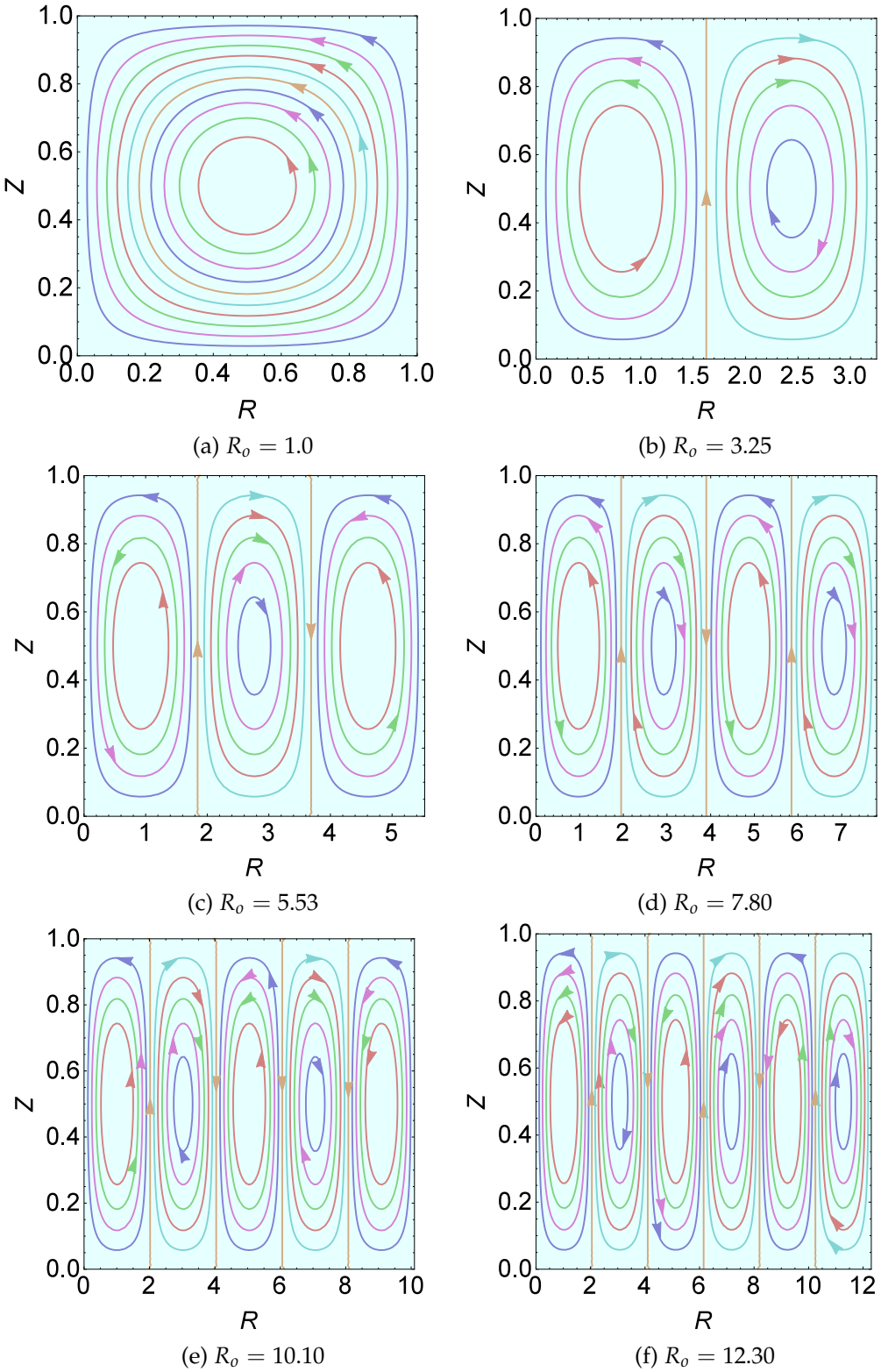

(a) $R_o = 1.0$ (b) $R_o = 3.25$

(c) $R_o = 5.53$ (d) $R_o = 7.80$

(e) $R_o = 10.10$ (f) $R_o = 12.30$

Figure 4. Plot of Ψ versus the breadth to height ratio, R, for different values of aspect ratio, R_o.

From the procedure outlined earlier in the case of the cylindrical RBC, for the finding of the critical Rayleigh number, Ra_c, it is apparent that compared to the problem of rectangular RBC, the cylindrical RBC problem involves a combination of Bessel and trignometric functions as the eigenfunction. Further, Ra_c is obtained by using a constrained extremisation approach like in the case of the rectangular RBC problem. The constraint in the case of rectangular RBC involves $\sin[p] = 0$ while the cylindrical RBC

Preprints (www.preprints.org) | NOT PEER-REVIEWED | Posted: 26 September 2023 doi:10.20944/preprints202309.1721.v1

case involves $J_1[p] = 0$. It is important to see the plots of $\sin[p]$ and $J_1[p]$ versus p in order to further understand the difference between the two problems.

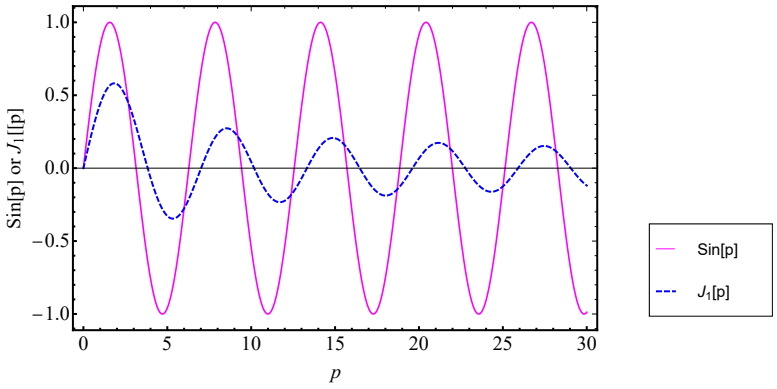

Figure 5. Plot of $Sin[p]$ and $J_1[p]$ versus p.

The periodicity of the *sine* function is 2π but we cannot define the same while dealing with Bessel functions since the wave-length, λ, depends on the range of R_o under consideration. Increase in the value of R_o results in a decrease in the value of the wave-length and also decrease in its amplitude. Such decreases in the wave-length happen only upto two pairs of counter-rotating cells. Beyond the 2^{nd} pair of counter-rotating cells, we observe that $\frac{d\lambda}{dR_o}$ becomes a constant, for values of $R_o > 13.3237$. The amplitude, $A(R_o)$, however, is such that $\frac{dA}{dR_o} < 0$. One more observation that can be made is that after every completion of a cycle by the constraint function $J_1[p]$, there will be appearance of an additional cell opposite in sense to the previous cell. This happens continuously in all range of values of R_o. Yet another observation that we can make is that in the range of values of R_o wherein the crest of the constraint function appears, we see one counter-rotating cell. Likewise we see clockwise-rotating cells in the trough region of such functions. This is true for both cylindrical and rectangular RBC problems.

The points at which the $J_1[p]$ curve crosses the $p-$axis gives us its root which is related to p_k. Hundred roots of $J_1[p] = 0$ were calculated to see if we could come up with some new observations. We found that $|p_{i+1} - p_i| \approx 3.1416(\text{nearly } \pi)$ for $i \geq 2$(after the second cell). This observation is in line with our findings on the nature of cells. We had mentioned earlier that cells beyond the second cell are symmetric in its horizontal dimension. This observation most importantly confirms that $|p_{i+1} - p_i|$, in fact, is the cell-width.

We next focus our attention on enclosures with moderate/large values of R_o. Our intention at this point is to find an analytical expression for the $p_i's$ as a function of k. This information is presented as tabulated values in Table 1. In order to find the expression of $p_k(k)$, we tried to fit a linear interpolation curve on the data of Table 1. The formulae that came to mind in obtaining the line of best fit are $p_0 + k\pi,\ p_1 + (k-1)\pi,\ p_2 + (k-2)\pi,\ p_3 + (k-3)\pi,\ p_4 + (k-4)\pi$, where $k = 1,\ 2,\ 3, \cdots$. As observed earlier, there is symmetry in the structure of the cells beyond the first-cell and hence quite expectedly the third function and onwards were found to be the lines of best fit. Though the fourth function and those beyond it produce least errors in the expression of $p_i(k)$ for large values of R_o compared to the third function, but these functions had large errors in them for smaller values of R_o. Hence we have chosen

$$p_k = p_2 + (k-2)\pi, (k = 1,\ 2,\ 3, \cdots) \tag{48}$$

as the line of best fit. On substituting p_k from equation (48), it was found that $o(J_1[p_k]) = 10^{-3}$, while the roots of $J_1[p]$ reported in Table 2 were found to be $o(10^{-6})$. This information is recorded in Table 2. This table indicates the difference in the accuracy of the zeros of $J_1[p] = 0$ obtained numerically and

Preprints (www.preprints.org) | NOT PEER-REVIEWED | Posted: 26 September 2023 doi:10.20944/preprints202309.1721.v1

by the derived formula. The roots given by equation (48) and the actual roots of $J_1[p]$, for different values of k, are plotted graphically in Figure 6. The figure clearly shows that the roots obtained from the formula (48) and the actual roots of $J_1[p]$(obtained numerically) coincide upto three decimal digits and is good enough for our purpose as shown in Figure 6.

Table 2. Roots of equation (44) obtained numerically and those by the analytical expression $p_k = p_2 + (k-2)\pi$(Eq. (48)).

k	p_k (actual roots)	$J_1[p_k] \times 10^6$	$p_k = p_2 + (k-2)\pi$	$J_1[p_k] \times 10^3$	% Error in p
1	3.83171	1.62304	3.87400	16.93522	0.01103
2	7.01559	0.99944	7.01559	0.00099	0.00000
3	10.17350	7.95682	10.15720	4.06964	0.00160
4	13.32370	1.76078	13.29880	5.44531	0.00186
5	16.47060	5.90396	16.44040	5.95002	0.00183
6	19.61590	7.47074	19.58200	6.10788	0.00172
7	22.76010	2.61132	22.72360	6.11099	0.00160
8	25.90370	4.37457	25.86510	6.04101	0.00149
9	29.04680	4.22349	29.00670	5.93627	0.00138
10	32.18970	2.82463	32.14830	5.81595	0.00128

5.4. Expression of the number of cells and the Rayleigh number as a function of the aspect ratio

On substituting p_k of equation (48) in the place of p in equation (43), we get

$$Ra(R_o, k(R_o)) = \frac{\left[\left(\frac{p_2+(k-2)\pi}{R_o}\right)^2 + \pi^2\right]^3}{\left(\frac{p_2+(k-2)\pi}{R_o}\right)^2}. \tag{49}$$

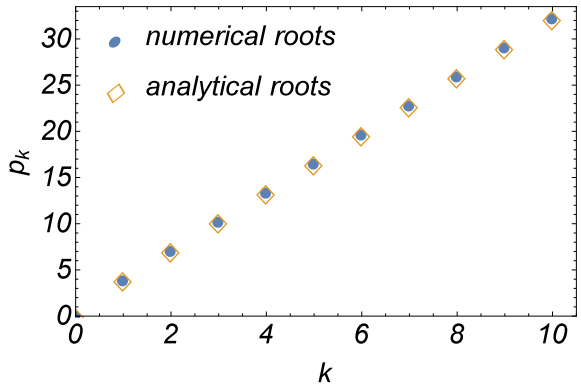

Figure 6. Roots of equation (44) obtained numerically and those obtained analytically by the relation $p_k = p_2 + (k-2)\pi$.

We know from Table 1 that k depends on R_o and that over a range of values of R_o, k remains the same. For example, for $R_o \in [0.8,\ 2.37)$ we have $k = 1$, and likewise for $R_o \in [2.37,\ 3.82)$ we have $k = 2$ and so on. This exact dependency of k on R_o is represented pictorially in Figure 7.

Preprints (www.preprints.org) | NOT PEER-REVIEWED | Posted: 26 September 2023 doi:10.20944/preprints202309.1721.v1

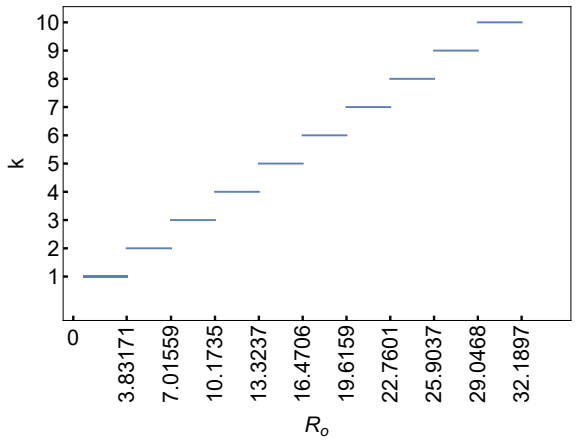

Figure 7. Plot of number of cells, k, versus R_o.

Using equation (49), we can determine Ra_c. A little explanation is required as to how exactly Ra_c is calculated. From Table 1, we can extract information on k for a given value of R_o and this yields us Ra_c for that assumed value of R_o. This procedure is followed for each value of R_o. Such a plot of Ra_c as a function of R_o is presented in Figure 8. The intersection points of the various marginal stability curves in Figure 8 provide information to us on the increment by 1 to the number of cells. Up to the first intersection point, the number of cells that manifest is one. From the first intersection point to the second, the number of cells that appear is 2. One can similarly make conclusion on k for the remaining values of R_o. The intersection point between two consecutive marginal stability curves give us information not only about what is documented in Table 1 but also provides vital information on the exact dependency of k on R_o(piecewise linear dependency as seen in Figure 7). To determine such an intersection point, we consider

$$\frac{\left[\left(\frac{p_2+(k-2)\pi}{R_o}\right)^2+\pi^2\right]^3}{\left(\frac{p_2+(k-2)\pi}{R_o}\right)^2}=\frac{\left[\left(\frac{p_2+(k-1)\pi}{R_o}\right)^2+\pi^2\right]^3}{\left(\frac{p_2+(k-1)\pi}{R_o}\right)^2}. \tag{50}$$

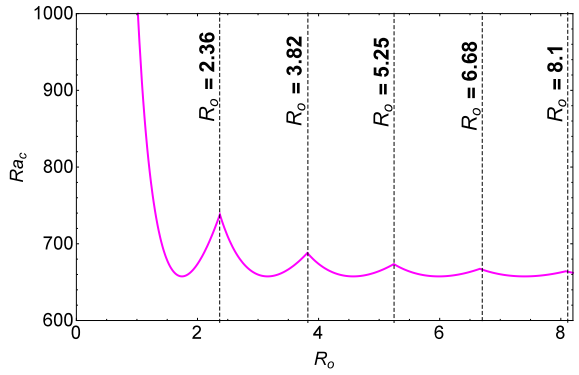

Figure 8. Plot of Ra_c as a function of R_o of the cylindrical enclosure.

On solving the equation (50) for k we obtain a 7^{th} degree polynomial equation whose real root helps us in determining the number of cells. The relationship between k and R_o may now be written by noting the following facts:

1. k is an integer.
2. The least number of cells is 1, i.e., $k \geq 1$.

Preprints (www.preprints.org) | NOT PEER-REVIEWED | Posted: 26 September 2023 doi:10.20944/preprints202309.1721.v1

On making use of the above 2 bits of information, the explicit expression of k in terms of R_o can be obtained as a root of the polynomial equation as

$$k = [Q_1] + \delta_{[Q_1]0}, \tag{51}$$

where

$$\left.\begin{aligned} Q_1 = q_1 + \sqrt{q_1^2 + \frac{q_2^2 + q_2\pi^2 q_3 + \pi^4\left(\pi^2 + 3\pi^2 R_o^2\right)^2}{6\pi^4 q_2}}, \\ q_1 = \frac{3\pi - 2p_2}{2\pi}, \\ q_2 = \sqrt[3]{\frac{q_4^2}{\pi^6 R_o^6} + 6\sqrt{3}\pi^3 q_4 + 27\pi^6\pi^6 R_o^6}, \\ q_3 = \left(18\pi p_2 - 13\pi^2 - 3\pi^2 R_o^2 - 6p_2^2\right), \\ q_4 = \sqrt{-27\pi^4\pi^{14} R_o^{10} - 9\pi^2\pi^{16} R_o^8 + \pi^{18}\left(-R_o^6\right)}. \end{aligned}\right\} \tag{52}$$

In equation (51), $[Q_1]$ is the ceil function of Q_1. We note here that the ceil function is a function which returns the smallest integer greater than or equal to Q_1. The term $\delta_{[Q_1]0}$ is the Kronecker delta function which returns 1 when $[Q_1]$ is equal to zero and returns 0 otherwise. The value of k gives the number of cells.

While obtaining Ra_c from equation (49), we have to determine p_c. With k as a function of R_o being explicitly known now through equation (51), we may directly determine p_c for a given R_o without seeking recourse to Table 1. So we now write

$$p_c = p_2 + (k-2)\pi, \tag{53}$$

where k is given by equation (51). With this definition of p_c, the expression of Ra_c, from equation (49), is now written as

$$Ra_c(R_o) = \frac{\left[\left(\frac{p_2+(k-2)\pi}{R_o}\right)^2 + \pi^2\right]^3}{\left(\frac{p_2+(k-2)\pi}{R_o}\right)^2}. \tag{54}$$

5.5. Expression of the wave number in a very shallow enclosure

Recalling that $\mathfrak{a}_c = \frac{p_c}{R_o}$, we may, on using equation (53), write it as

$$\mathfrak{a}_c = \frac{p_2 + (k-2)\pi}{R_o}. \tag{55}$$

This definition is obviously applicable for very shallow enclosures and is the expression of the critical wave number. As noted earlier the symmetry in the structure of the cell is observed beyond the 2^{nd} cell. The radial distance between the axis of the cylinder and the edge of the 2^{nd} cell is $\frac{p_2}{\mathfrak{a}_c}$. All pairs of counter-rotating cells after the 2^{nd} cell have approximately the wave-length of $\frac{2\pi}{\mathfrak{a}_c}$. The exactness of the representation of the wave-length improves if we take R_o large enough. Figure 9 is the plot of streamlines in the region $R \in \left[0, \frac{p_2+2\pi}{\mathfrak{a}_c}\right]$. The Figure 9 clearly shows that the region $\left[0, \frac{p_2}{\mathfrak{a}_c}\right]$ includes the stagnant zone and the first counter-clockwise rotating cell. The region $\left[\frac{p_2}{\mathfrak{a}_c}, \frac{2\pi}{\mathfrak{a}_c}\right]$ represents the wave-length. Expectedly, for very large values of R_o the boundary effects(curvature effects) become

Preprints (www.preprints.org) | NOT PEER-REVIEWED | Posted: 26 September 2023 doi:10.20944/preprints202309.1721.v1

negligible and hence in that case $\mathfrak{a}_c$ converges to the value $\frac{\pi}{\sqrt{2}}$ which is the wave number of the classical rectangular *RBC* problem. In this case, $Ra_c = \dfrac{27\pi^4}{4}$.

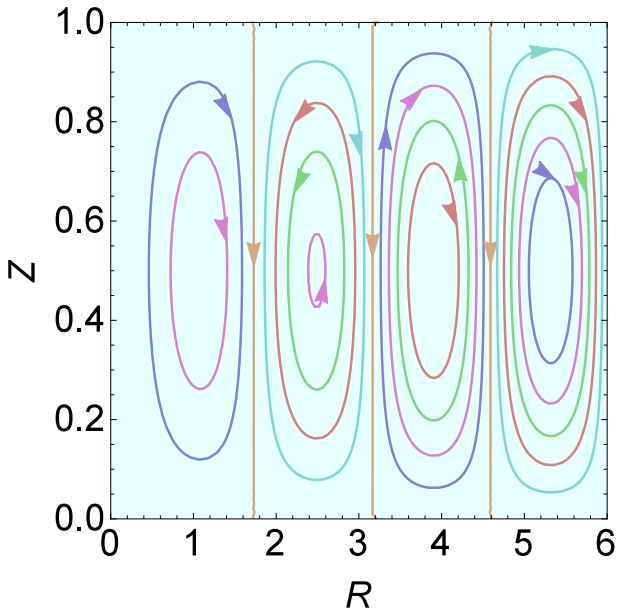

Figure 9. Plot of Ψ versus R in the region $\left[0,\ \frac{p_2+2\pi}{\mathfrak{a}_c}\right]$.

We next discuss aspects of the two-dimensional rectangular *RBC* problem similar to those of the cylindrical counter part.

5.6. Results on the rectangular RBC problem

Following the procedure of the cylindrical *RBC* problem, we now present the results of the rectangular *RBC* problem. The stream function in this case is given by:

$$\psi = \frac{\mathcal{A}}{\pi^3}\frac{k_c/R_o}{\left[(k_c/R_o)^2+1\right]^2} Ra \sin\left[\frac{k_c}{R_o}\pi R\right]\sin[\pi Z]. \tag{56}$$

The relation connecting the number of cells and the aspect ratio in the case of the rectangular *RBC* is:

$$k = [Q_2] + \delta_{[Q_2]0}, \tag{57}$$

where

$$\left.\begin{aligned} Q_2 &= \frac{1}{2}\left[-1+\sqrt{1-\frac{2}{3}\left(1+3R_o^2-\frac{(1+3R_o^2)^2}{q_5}-q_5\right)}\right], \\ q_5 &= -1-9R_o^2-27R_o^4+27R_o^6+6\sqrt{3}\,q_6, \\ q_6 &= \sqrt[3]{-R_o^6(1+9R_o^2+27R_o^4)}. \end{aligned}\right\} \tag{58}$$

In equation (57), $[Q_2]$ is the ceil function of Q_2 and $\delta_{[Q_2]0}$ is the Kronecker delta function. The value of k represents the number of cells and this then determines $\mathfrak{a}_c$.

We next present the similarities and the differences between the results of the cylindrical and rectangular *RBC* problems.

Preprints (www.preprints.org) | NOT PEER-REVIEWED | Posted: 26 September 2023 doi:10.20944/preprints202309.1721.v1

5.7. Similarities and differences between the results of the cylindrical enclosure(CE) and the rectangular enclosure(RE)

Though the two geometries are different they possess many similarities. Some of them are

- The wave number as well as the critical Rayleigh number of both CE and RE for $R_o \gg 1$ are almost equal to $\frac{\pi}{\sqrt{2}}$ and $\frac{27\pi^4}{4}$ respectively.
- Each new Rayleigh-Bénard cell(RB cell) in CE/RE always appears close to the lateral boundaries(right lateral boundary in RE).
- A new cell forms in CE/RE with an approximate increase of 1.42 in the value of R_o.

Differences between the results of the two problems are:

- The eigenfunctions in the case of RE are always trigonometric while in the case of CE, they involve Bessel functions as well.
- The rolls are straight in RE while they are circular in CE.
- In cylindrical RB cell there exists a stagnant region and the same is not seen in the case of RE.
- Due to the presence of a stagnant region, the dependence of the number of cells on the aspect ratio is not the same in the cases of CE and RE.
- As the value of R_o is increased, the horizontal dimension of the streamlines does not change while the vertical dimension gradually increases towards the lateral surface of the cylinder. In the RE the cell aspect ratio is always fixed while it is not so in CE.
- Critical values of the wave number and Rayleigh number are not the same in the cases of CE and RE for small/moderate values of R_o.

6. Conclusion

The present investigation is an analytical study of RBC in CE/RE. The minimal Fourier series is employed to obtain analytical results for Ra_c, $\mathfrak{a}_c$ and the number of cells, k, as a function of R_o. The onset of convection is predicted theoretically using the linear stability analysis. The nature of the cells and the number of cells are investigated for various values of R_o by plotting the stream function. In the plots of CE, we observe that the first cell forms away from its axis and closer to its lateral surface. A stagnant region is observed around the axis of the cylinder. Such a positioning of the first cell is seen for all values of R_o. In view of the difference in the positioning of the first cell in the case of CE we introduced the concept of cell-width for small/moderate values of R_o and the concept of wave number for $R_o \gg 1$. For values of moderate and large values of R_o, we observe a symmetry in the width of the cells but the cell aspect ratio is different. An explicit expression for the number of cells as a function of R_o in both CE and RE can be written out as reported in the paper. Similarly, an expression for Ra_c as a function of R_o can be obtained. In the case of $R_o \gg 1$, $\mathfrak{a}_c = \frac{\pi}{\sqrt{2}}$ and $Ra_c = \frac{27\pi^4}{4}$. These findings in both CE and RE are rather new and informative.

- For the first time in the literature, analytical solutions are obtained for the RBC in cylindrical enclosure.
- The problems of cylindrical and rectangular enclosures are uniquely handled using the curvature parameter.
- The fundamental details on the formation and nature of the cells are clearly brought out by plotting the streamlines for different values of aspect ratios.
- Two different ranges of aspect ratios are defined where the concept of cell-width and the wave number are individually applicable.
- A new function, $p = 7.01559 + (k-2)\pi$, $(k = 1, 2, 3, \cdots)$ is invented as a solution to the Bessel function of first kind and first order, $J_1[p] = 0$, which yields the solution with $o(10^{-3})$ accuracy.
- An explicit expression connecting the number of cells and the aspect ratio is found. From this, for enclosure of any given aspect ratio one can theoretically predict the number of cells that manifests. Also, for a given aspect ratio, we can directly found the onset of convection.

- For a very shallow enclosures, it is shown that the curvature effects becomes negligible and hence the results of CE coincides with the results of classical RBC problem in RE.

All the results discussed above are also applicable in the case of rectangular enclosures.

Author Contributions: All authors contributed equally to analyzing the data, reaching conclusions, and writing the paper. All authors have read and agreed to the published version of the manuscript.

Institutional Review Board Statement: Not applicable.

Informed Consent Statement: Not applicable

Data Availability Statement: Not applicable.

Acknowledgments: Authors are grateful to the University of Tarapacá for supporting her research.

Conflicts of Interest: Authors declare no conflict of interest.

Abbreviations

The following abbreviations are used in this manuscript:

CE	Cylindrical enclosure
RBC	Rayleigh-Bénard convection
RE	Rectangular enclosure

References

1. Moore, D.R.; Weiss, N.O. Two-dimensional Rayleigh-Bénard convection. *J. Fluid Mech.* **1973**, *58*, 289–312.
2. Bergé, P.; Dubois, M. Rayleigh-Bénard convection. *Contemp. Phys.* **1984**, *25*, 535–582.
3. Roche, P.E.; Castaing, B.; Chabaud, B.; Hébral, B.; Sommeria, J. Side wall effects in Rayleigh Bénard experiments. *Eur. Phys. J. B* **2001**, *24*, 405–408.
4. Stevens, R.J.; Lohse, D.; Verzicco, R. Sidewall effects in Rayleigh–Bénard convection. *J, Fluid Mech.* **2014**, *741*, 1–27.
5. Wen, B.; Ding, Z.; Chini, G.P.; Kerswell, R.R. Heat transport in Rayleigh–Bénard convection with linear marginality. *Phil. Trans. A* **2022**, *380*, 20210039.
6. Liang, S.F.; Vidal, A.; Acrivos, A. Buoyancy-driven convection in cylindrical geometries. *J. Fluid Mech.* **1969**, *36*, 239–258.
7. Stork, K.; Müller, U. Convection in boxes: an experimental investigation in vertical cylinders and annuli. *J. Fluid Mech.* **1975**, *71*, 231–240.
8. Charlson, G.S.; Sani, R.L. Thermoconvective instability in a bounded cylindrical fluid layer. *Int. J. Heat Mass Transfer* **1970**, *13*, 1479–1496.
9. Koschmieder, E. On convection on a uniformly heated plane. *Beitr. Phys. Atmos.* **1966**, *39*.
10. Koschmieder, E. On convection on a uniformly heated rotating plane. *Beitr. Phys. Atmos.* **1967**, *40*, 216–225.
11. Koschmieder, E. On the wavelength of convective motions. *J. Fluid Mech.* **1969**, *35*, 527–530.
12. Charlson, G.S.; Sani, R.L. On thermoconvective instability in a bounded cylindrical fluid layer. *Int. J. Heat Mass Transfer* **1971**, *14*, 2157–2160.
13. Hébert, F.; Hufschmid, R.; Scheel, J.; Ahlers, G. Onset of Rayleigh-Bénard convection in cylindrical containers. *Phys. Rev. E* **2010**, *81*, 046318–1–046318–11.
14. Wang, B.F.; Ma, D.J.; Chen, C.; Sun, D.J. Linear stability analysis of cylindrical Rayleigh–Bénard convection. *J. Fluid Mech.* **2012**, *711*, 27–39.
15. Yu, J.; Goldfaden, A.; Flagstad, M.; Scheel, J.D. Onset of Rayleigh-Bénard convection for intermediate aspect ratio cylindrical containers. *Phys. Fluids* **2017**, *29*, 024107–1–024107–10.
16. Li, P.X.; Li, B.W.; Chen, L.; Leng, X.Y.; Luo, X.H.; Yu, Y.; Zhang, J.K. 3D DNS of laminar Rayleigh-Bénard convection in a cylinder for incompressible fluid flow. *Chinese J. Phys.* **2022**, *79*, 374–394.
17. Zebib, A. Onset of natural convection in a cylinder of water saturated porous media. *Phys. Fluids* **1978**, *21*, 699–700.
18. Bau, H.H.; Torrance, K.E. Onset of convection in a permeable medium between vertical coaxial cylinders. *Phys. Fluids* **1981**, *24*, 382–385.

19. Haugen, K.B.; Tyvand, P.A. Onset of thermal convection in a vertical porous cylinder with conducting wall. *Phys. Fluids* **2003**, *15*, 2661–2667.
20. Bringedal, C.; Berre, I.; Nordbotten, J.M.; Rees, D.A.S. Linear and nonlinear convection in porous media between coaxial cylinders. *Phys. Fluids* **2011**, *23*, 094109–1–094109–11.
21. Barletta, A.; Storesletten, L. Onset of convection in a vertical porous cylinder with a permeable and conducting side boundary. *Int. J. Therm. Sci.* **2015**, *97*, 9–16.
22. Siddheshwar, P.G.; Lakshmi, K.M. Darcy-Bénard convection of Newtonian liquids and Newtonian nanoliquids in cylindrical enclosures and cylindrical annuli. *AIP Phys. Fluids* **2019**, *31*, 084102–1–084102–19.
23. Bodenschatz, E.; Pesch, W.; Ahlers, G. Recent developments in Rayleigh-Bénard convection. *Annu. Rev. Fluid Mech.* **2000**, *32*, 709–778.
24. Wen, B.; Goluskin, D.; LeDuc, M.; Chini, G.P.; Doering, C.R. Steady Rayleigh–Bénard convection between stress-free boundaries. *J. Fluid Mech.* **2020**, *905*, R4.
25. Shishkina, O. Rayleigh-Bénard convection: The container shape matters. *Phys. Rev. Fluids* **2021**, *6*, 090502.
26. Ecke, R.E.; Shishkina, O. Turbulent rotating Rayleigh–Bénard convection. *Annu. Rev. Fluid Mech.* **2023**, *55*, 603–638.